Simulation of a model microswimmer



2009 J. Phys.: Condens. Matter 21 204101

(http://iopscience.iop.org/0953-8984/21/20/204101)

IOP PUBLISHING JOURNAL OF PHYSICS: CONDENSED MATTER

J. Phys.: Condens. Matter **21** (2009) 204101 (6pp) doi:10.1088/0953-8984/21/20/204101

# Simulation of a model microswimmer

**Matthew T Downton and Holger Stark**

Institut für Theoretische Physik, Technische Universität Berlin, Hardenbergstraße 36, D-10623 Berlin, Germany

Received 26 November 2008, in final form 10 January 2009
Published 21 April 2009
Online at stacks.iop.org/JPhysCM/21/204101

**Abstract**

We discuss the modelling of a microswimmer that operates in a 'squirmer' mode, by means of stochastic rotation dynamics. The squirmer that we model can easily be tuned between a 'pusher' and a 'puller'. We examine the flows produced by the squirmer and find that there is good agreement between both the predicted and simulated velocities of locomotion and the resulting flow field.

(Some figures in this article are in colour only in the electronic version)

## 1. Introduction

Swimming at low Reynolds number is a subject of great interest because microorganisms, due to their small size, must adapt to an environment in which viscous forces dominate over inertial forces. In this case, the reversal of forces acting on the fluid, e.g., through the no-slip boundary condition, leads to reversal of the induced fluid flow. Any swimming mechanism of an isolated object must therefore be non-reciprocal [1].

One solution that organisms such as Paramecium adopt is to beat filaments known as cilia which cover their entire outer surface. These filaments have a complex internal structure and display a variety of different beating patterns that can be synchronized with wavelength of order 5–10 filament spacings [2]. Because the number of such filaments is high, simplified models are required in order to be able to theoretically model such organisms. Various models have been implemented that have varying resolution. One such treatment is to consider the organism a simple geometrical shape such as a sphere and consider wavelike deformations of the outer surface [3, 4]. The motivation for this approximation is that the tips of the cilia make a continuous surface that covers the organism. These so-called 'squirmers' have attracted some interest recently as they allow pairs [5] and collections [6] of interacting microswimmers to be simulated. These studies have taken the limit of a purely tangential surface velocity whereas the original model included provisions for both tangential and radial velocities. There is also the possibility that some microorganisms may swim directly through deformations of the cell membrane [7, 8].

A range of numerical techniques can be used to study low Reynolds number swimmers. In the limit of zero Reynolds number, the long-range effects of hydrodynamics can be included into models that treat the fluid implicitly. The squirmer that is the focus of the current work has been simulated using the Stokesian dynamics method [5, 6]. This formalism, based on the Oseen tensor and mobilities derived from it, has also been used to study magnetoelastic filaments [9] and the swimming of *Spiroplasma* [10]. Alternatively, for slender filaments, an anisotropic friction coefficient can be used [11, 12]. These techniques have varying degrees of accuracy and are by and large straightforward and efficient to implement for small systems. One limitation, however, is the difficulty with which complex geometries can be studied.

This problem is not serious for several modern simulation methods that explicitly model the fluid. The mesoscopic lattice-Boltzmann method [13] has been used to study the three link swimmer of Najafi and Golestanian [14]. The swimming of sperm cells and synchronization of cilia was simulated with multi-particle collision dynamics [15].

So far there have only been a few studies of low Reynolds number swimmers that explicitly include thermal fluctuations. Earl *et al* considered the three link swimmer and an elastic filament using multi-particle collision dynamics [13] and Lobaskin *et al* have considered the Brownian motion of a swimmer using the lattice-Boltzmann method [16]. In the following paper we discuss the implementation of a squirmer driven by a prescribed velocity field on the surface of a sphere using multi-particle collision dynamics. Section 2 gives details of the simulation technique. This is followed by a set of results in section 3. Finally there is a short conclusions section.

## 2. Model details

The microswimmer that we consider here is driven by a purely tangential distortion on the outer surface of a 'colloidal' particle of radius $a$. The velocity at a point $\mathbf{r}_s$ on the surface is

 

given by the expression [6]:

$$\mathbf{v}_s(\mathbf{r}_s, \hat{\mathbf{e}}) = \sum_{n=1}^{2} \frac{2}{n(n+1)} B_n \left( \frac{\hat{\mathbf{e}} \cdot \mathbf{r}_s}{a} \frac{\mathbf{r}_s}{a} - \hat{\mathbf{e}} \right) P_n'(\hat{\mathbf{e}} \cdot \mathbf{r}_s/a), \quad (1)$$

where the $B_n$ are constants, $P_n'(x)$ is the derivative of the $n$th Legendre polynomial, and $\hat{\mathbf{e}}$ is a unit direction vector associated with the sphere. From equation (1) one immediately calculates the polar velocity component in spherical coordinates, $u_\theta = B_1 \sin\theta + (B_2/2)\sin 2\theta$, where $\theta = \arccos(\hat{\mathbf{e}} \cdot \mathbf{r}_s/a)$ is the polar angle. For this model the velocity of the colloid in the direction $\hat{\mathbf{e}}$ is determined from the fact that the total force acting on the swimmer is zero and amounts to $2B_1/3$ [4, 5]. The second parameter, $B_2$, changes the characteristics of the distortion, see figure 1. For $\beta \equiv B_2/B_1 < 0$, the propulsion acts from the rear of the object (similar to biological swimmers—pushers); if $\beta > 0$ then the propulsion acts from the front of the swimmer—pullers. The analytic form of the resulting flow field for a single squirmer can be calculated analytically and is reproduced in appendix.

To model the solvent, we use the stochastic rotation dynamics (SRD) algorithm [17], a molecular dynamics method for effective fluid particles that can be used to efficiently simulate hydrodynamic solvent modes. The algorithm can be easily modified so that external objects can be incorporated within the simulation [18], with the result that simulations can be performed on systems of objects immersed in a bath with which momentum and thermal energy can be exchanged. Implementation of SRD is straightforward and the technique has the advantage that the transport coefficients of the fluid can be calculated analytically [19, 20]. The SRD fluid consists of an ideal gas of particles that undergo periodic 'collisions'. During a collision, the simulation box is divided into cubic cells of dimension $h \times h \times h$. The velocity of the centre of mass, $\mathbf{v}_{cm}$, of particles contained within each cell is calculated and the velocity of each particle with respect to $\mathbf{v}_{cm}$ is then rotated by an angle $\alpha$ around an axis chosen at random. The new velocity for the $i$th particle is given by

$$\mathbf{v}_i' = \mathbf{v}_{cm} + \mathbf{R}[\mathbf{v}_i - \mathbf{v}_{cm}], \quad (2)$$

where $\mathbf{R}$ is a rotation matrix. Between collisions, the particles stream forward along straight trajectories for a time $\delta t$

$$\mathbf{r}_i(t + \delta t) = \mathbf{r}_i(t) + \delta t \mathbf{v}_i(t). \quad (3)$$

The collision step conserves the momentum and kinetic energy of the cell particles while the streaming step transfers momentum between cells. These two components are sufficient to create a dynamical system that satisfies the Navier–Stokes equation with the rotation angle, $\alpha$, streaming time, $\delta t$, and mean cell occupancy, $\gamma$, determining the solvent transport coefficients [19, 20]. We note that there are variations of this collision rule that allow the angular momentum of the cell to be conserved [21].

To implement a non-slip boundary on the surface of the colloid/squirmer we follow the implementation of [22] with some minor modifications. During the streaming step collisions between the colloid and solvent particles are identified. At each collision, a new random thermal velocity for the solvent particle is chosen relative to the velocity of the contact point on the colloid surface:

$$\mathbf{v}_{contact} = \mathbf{v}_c + \mathbf{v}_s(\mathbf{r} - \mathbf{r}_c, \hat{\mathbf{e}}) + \boldsymbol{\Omega} \wedge (\mathbf{r} - \mathbf{r}_c), \quad (4)$$

where $\mathbf{r}$ is the collision point, the colloid position, velocity and angular velocity are $\mathbf{r}_c$, $\mathbf{v}_c$ and $\boldsymbol{\Omega}$, and $\mathbf{v}_s$ is the prescribed velocity from equation (1). The tangential and normal components of the random thermal velocity for the colliding particle are chosen from the distributions $p(v) \propto \exp(-mv^2/2k_BT)$ and $p(u) \propto u\exp(-mu^2/2k_BT)$ respectively. The velocity and rotational velocities of the colloid are then set so that the linear and angular momentum of the colloid–particle pair before and after the collision are conserved. In this way fluctuations of both the rotational and translational degree of freedom of the colloid can be simulated.

The colloidal particle overlaps with the cells that are used in the SRD simulation. We follow previous work that attempted to reduce slip on boundaries and fill the colloid with particles at random positions [21, 23], which are newly chosen before each collision step. The particles are given the velocity of the colloid surface at the same polar angle $\theta = \arccos(\hat{\mathbf{e}} \cdot \mathbf{r}_s/a)$ and then participate in the SRD collision process with all the particles within one cell. The colloid is given the change in momentum that occurs during this step for the particles filling the colloid. Of the variations in boundary conditions that we tried, we found that this gave the closest agreement with the theoretical prediction of the squirmer velocity. The relevant values of the simulation parameters that we use are given in table 1.

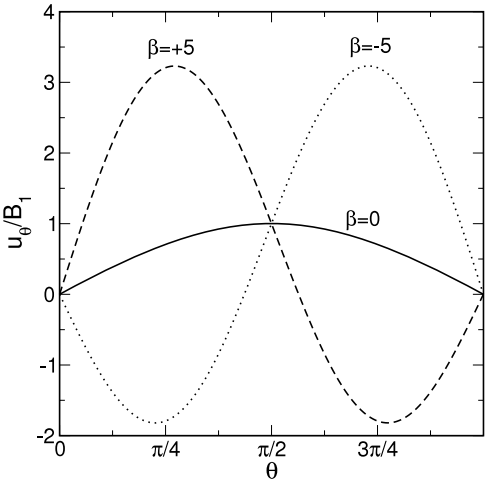


**Figure 1.** Polar velocity on the surface of the squirmer.

## 3. Results

Short, independent simulations of the model presented in section 2 were performed for a number of different values of $B_1$ in order to calculate the time average velocity $v = \langle \hat{\mathbf{e}} \cdot \mathbf{v}_c \rangle$. The results of these are shown in figure 2(a). The velocity is linear in $B_1$ with a slope of $0.601 \pm 0.001$ for sets I–II and $0.639 \pm 0.001$ for set III. This compares favourably with the exact value of $2/3$ and represents a reasonable value for

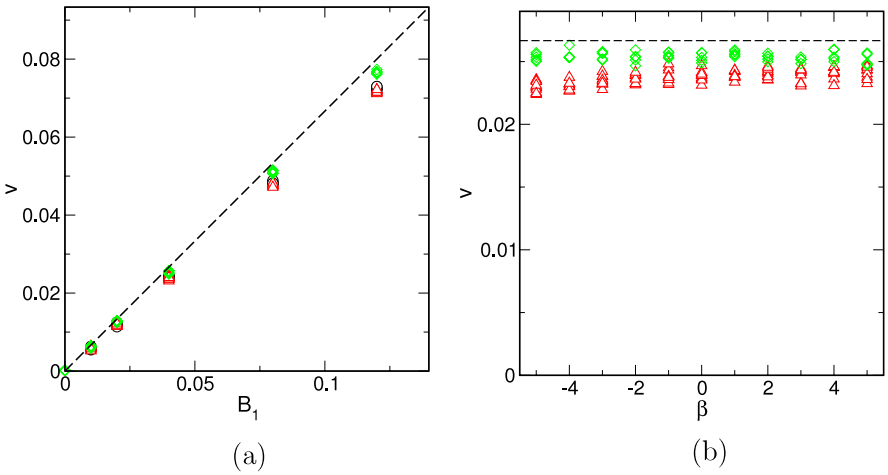


**Figure 2.** Simulation results for the velocity of the squirmer. Each point represents the result from a different independent simulation. The dashed lines indicate the predicted value (a) variation of the swimming speed $\langle \hat{\mathbf{e}} \cdot \mathbf{v}_c \rangle$ with $B_1$, parameter sets I (○), II (△) and III (◇), (b) variation of speed with $\beta$ for $B_1 = 0.04$, parameter set II (△) and III (◇).

**Table 1.** Parameters for the SRD fluid and the colloidal particle. Units are chosen such that $k_B T = 1$, $h = 1$ and $m = 1$, time is measured in units $h\sqrt{m/k_B T}$. The colloid mass is taken to be the same as the mass of solvent particles that it displaces.

| Parameter | Set I | Set II | Set III |
|---|---|---|---|
| Mean occupancy per collision cell, $\gamma$ | 5 | 5 | 5 |
| Rotation angle, $\alpha$ | $\pi/2$ | $2\pi/3$ | $2\pi/3$ |
| Collision length, $\lambda = \delta t / h\sqrt{k_B T/m}$ | 0.1 | 0.02 | 0.02 |
| Kinematic viscosity, $\nu$ | 0.5 | 3.350 | 3.350 |
| Number of cells along each axis, $n$ | 24 | 24 | 60 |
| Squirmer radius, $a/h$ | 4 | 4 | 10 |

the coarse grained technique that we use. It also indicates the possibility that increasing the ratio of the squirmer radius to the collision cell size, $h$, may be helpful in increasing the accuracy of the simulations. The linearity holds over the range of Reynolds numbers studied (up to a maximum $Re = vr/\nu \approx 0.23$).

In figure 2(b) the variation of $v$ is plotted against $\beta$ for $B_1 = 0.04$. As expected, there is almost no variation across the range of $\beta$ studied for set III. The results for set II are however not in such good agreement, with a noticeable reduction in the velocity for $\beta < 0$. The cause of this asymmetry is not clear, though is likely to be due to the fact that the smaller colloid radius reduces the accuracy of the simulation.

In figure 3 velocity field profiles are shown for $\beta = 0$ and $\pm 5$. The tangential velocity on the surface of the squirmer is given by $u_\theta = B_1 \sin(\theta)(1 + \beta \cos(\theta))$. Therefore for $|\beta| > 1$ there is a section of the surface that has surface velocity in the direction opposite to the motion and as a consequence there will be flow in the direction opposite to $\hat{\mathbf{e}}$. This flow can be seen for $\beta = \pm 5$. Also noticeable for the larger values of $\beta$ is the formation of a ring vortex close to the pole and a maximum in the tangential velocity on the opposite hemisphere. The complete extent of the simulation box is shown in these plots and it is apparent the box is not large enough to capture the full $1/r^2$ decay of the flow field that is predicted by equation (A.1) for the cases $\beta = \pm 5$. For $\beta = 0$ the flow field is less long range since it decays as $1/r^3$. The power consumed by the swimmer to propel itself through the fluid amounts to $P/P_0 = 2(1 + \beta^2/2)$, where $P_0 = 6\pi\eta a v^2$ is the power one would need to drag a particle with the swimmer's velocity $v$ and size through the fluid [4]. It can, for example, be calculated from the power dissipated by the fluid flow. The longer range of the fluid field for $\beta \neq 0$ and the ring vortices result in an increased power consumption. Interestingly, the minimum power consumption for a squirmer with $\beta = 0$ is just twice the one of a passive particle.

Comparisons with the analytic flow field given in equation (A.1) are shown in figure 4. Overall, this field is well reproduced for $\beta = 0$, for $\pm 5$ however, there are significant deviations fore and aft of the squirmer in the regions where the velocity field takes on its maximum value. There are two systematic contributions to the error in the simulated flow field. First, for $|\beta| = 5$, the spatial variation in the driving flow on the boundary of the colloid (shown in figure 1) is large in comparison with the cell size used in the simulation algorithm. Second, as described above, the flow field has a long-range character for $|\beta| > 0$ and finite size effects due to the limited box size affect the results. Improvements can therefore be made by either increasing the ratio of the squirmer radius to the cell size, $a/h$, or by increasing the number of simulation cells, $n$. We find that flow fields generated using parameter set III more accurate than those shown in figure 4.

Although the method we have used to model the squirmer matches the predictions for the translational velocity, we have not yet explored the effects of thermal fluctuations on the colloid. We present briefly some initial results. First we note that the mean squared value of the angular frequency does not give a value in agreement with the equipartition theorem and we find a value of $\langle \boldsymbol{\Omega}(t) \cdot \boldsymbol{\Omega}(t) \rangle$ that is approximately six times the expected value, see figure 5(a)[1]. This is due to the

[1] We can exploit the linearity of solutions to the Stokes equations to view the rotation and translation of the squirmer as two independent problems: translation of a squirmer with the surface velocity given by equation (1) and rotation of a colloid with a no-slip boundary condition. In the latter problem there will be no rotation except through thermal fluctuations and we therefore expect the equipartition theorem to hold.

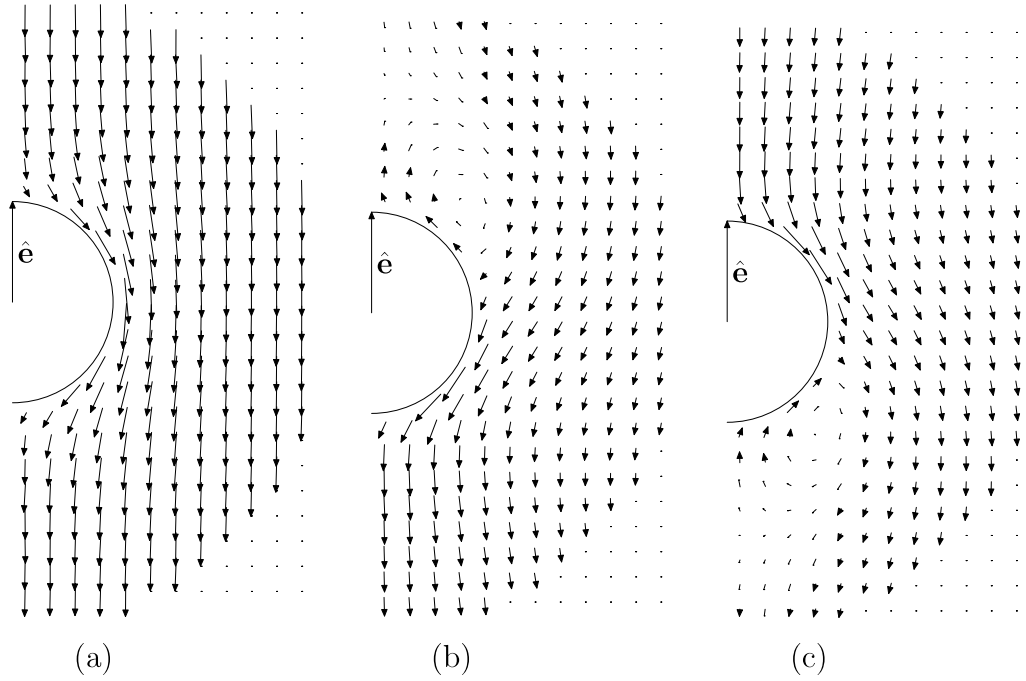


**Figure 3.** Flow field around the squirmer in the frame of the moving colloid, parameter set II, $B_1 = 0.04$ (a) $\beta = 0$, (b) $\beta = -5$, (c) $\beta = +5$.

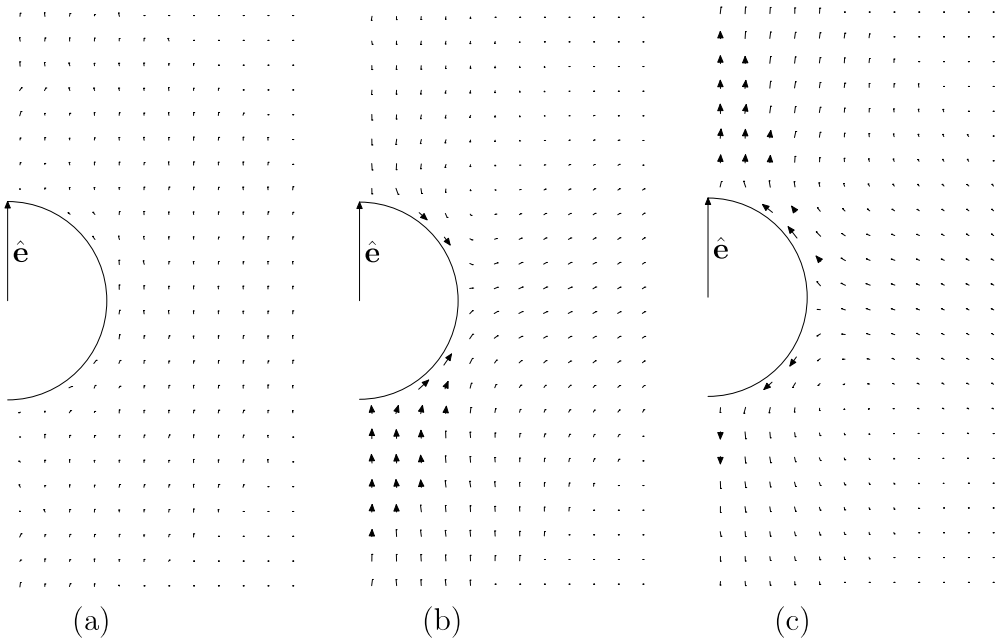


**Figure 4.** Difference between the flow field shown in figure 3 and the analytic velocity given in equation (A.1) (a) $\beta = 0$, (b) $\beta = -5$, (c) $\beta = +5$.

additional particles that are placed within the colloid, and a separate set of results shows that this discrepancy disappears if we remove these particles from the simulation (see the thick dark line in figure 5(a)). However, we note that in this latter case the mean translational velocity takes approximately half the value of the analytic theory.

The rotation of $\hat{\mathbf{e}}$ with time means that the path taken by the squirmer is that of a persistent random walk with persistence time $\tau$ given by the time required for the autocorrelation function $\langle \hat{\mathbf{e}}(t) \cdot \hat{\mathbf{e}}(0) \rangle$ to decay to $1/e$, see figure 5(b). This characteristic time is related to the rotational diffusion coefficient, $D_r$, by $\tau = 1/2D_r$ [24]. We find $\tau$ is the same for all values of $B_1$ and $\beta$ within a given parameter set. Taking $\langle \hat{\mathbf{e}}(t) \cdot \hat{\mathbf{e}}(0) \rangle = \exp(-t/\tau)$ and using $\mathbf{r}(t) = \mathbf{r}(0) + v \int_0^t \mathrm{d}t' \hat{\mathbf{e}}(t')$ it is possible to show that the mean squared displacement has the form

$$\left\langle |\mathbf{r}(t) - \mathbf{r}(0)|^2 \right\rangle = 2v^2\tau t - 2v^2\tau^2(1 - \exp(-t/\tau)). \quad (5)$$

A similar analysis has been performed on the trajectories of self-propelling chemical colloids [25]. A comparison between

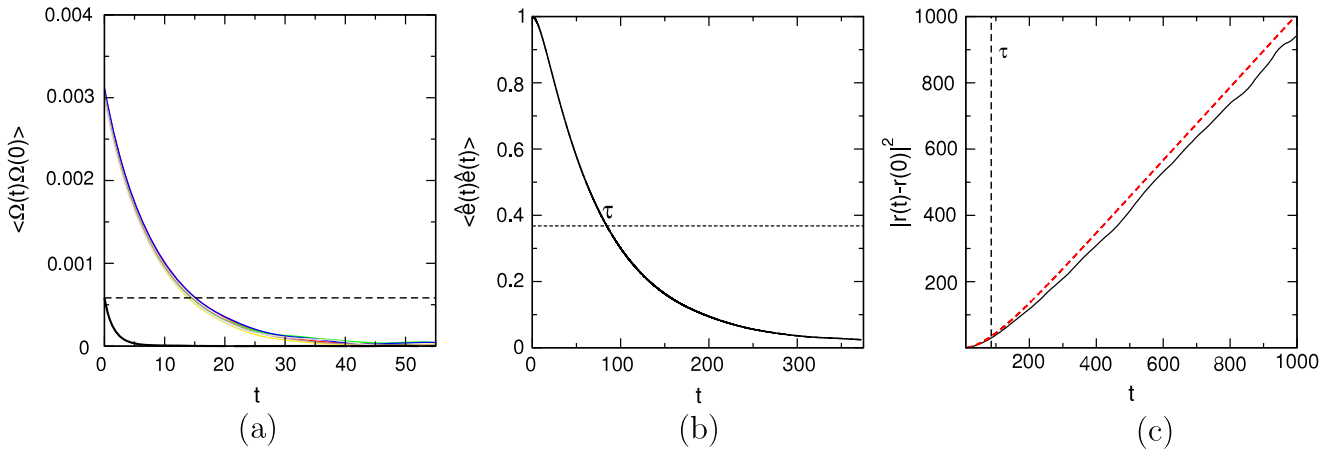


**Figure 5.** Effect of the orientational degree of freedom on the path taken by the colloid. (a) Autocorrelation function of the colloid angular velocity, $\langle \boldsymbol{\Omega}(t) \cdot \boldsymbol{\Omega}(0) \rangle$. The dashed line indicates the value $3k_BT/I$ expected from equipartition theory for a colloid with moment of inertia $I$ at equilibrium with a heat bath. The upper curves represents different values of $B_1$ in the range 0.01–0.12 for parameter set II; the lower curve is for a simulation where solvent particles within the colloidal particle are not included in the SRD collision step. (b) Autocorrelation function of the squirmer orientation, $\langle \hat{\mathbf{e}}(t) \cdot \hat{\mathbf{e}}(0) \rangle$; the decay time $\tau$ is indicated (same data as (a)). (c) Comparison between the simulated (solid line) and analytic (thick dashed line; $v = 2B_1/3$) mean squared displacements ($B_1 = 0.12$, parameter set II; vertical dashed line indicates $\tau$).

the simulated value of $\langle |\mathbf{r}(t) - \mathbf{r}(0)|^2 \rangle$ and equation (5) is shown in figure 5(c). For long times, the trajectory is diffusive and $\tau$ sets the crossover time from ballistic (i.e. $\propto t^2$) to linear scaling of the mean squared displacement. This change can be seen in the pronounced bend of $|\mathbf{r}_c(t) - \mathbf{r}_c(0)|^2$ close to a time in agreement with $\tau$. One cause of the systematic discrepancy between equation (5) and the measured value is the fact that the squirmer velocity is slightly less than $2B_1/3$ for parameter set II.

## 4. Conclusions

We have presented an implementation of a microswimmer using the stochastic rotation dynamics algorithm. We have found that the technique correctly yields the predicted velocity for a given set of input parameters and that flow field around the squirmer can be tuned so that the majority of the propulsive force comes from either the front or the back of the squirmer. Future studies of the method might include examination of the influence that no-slip boundaries, for instance in a slab geometry, have on the orientation and velocity of the particle.

## Acknowledgments

We acknowledge financial support from the Deutsche Forschungsgemeinschaft under grant no. Sta 352/7-1 and would like to thank the Mathematics department a TU-Berlin for access to computer facilities. J T Padding is thanked for helpful advice.

## Appendix. Flow field

The analytic form for the fluid velocity can be found in the literature [4, 5]. To keep this paper self-contained we repeat these formulae here for a frame that leaves the fluid at infinity at rest. The velocity of the fluid at a position $\mathbf{r}$ measured from the centre of the squirmer is

$$\begin{aligned}\mathbf{v}_{\text{fluid}} = {} & B_1 \left(\frac{a}{r}\right)^3 \left(\frac{\hat{\mathbf{e}}\cdot\mathbf{r}}{r}\frac{\mathbf{r}}{r} - \frac{\hat{\mathbf{e}}}{3}\right) \\ & + \frac{1}{2}\left(\left(\frac{a}{r}\right)^4 - \left(\frac{a}{r}\right)^2\right) B_2 P_2\left(\frac{\hat{\mathbf{e}}\cdot\mathbf{r}}{r}\right)\frac{\mathbf{r}}{r} \\ & + \left(\frac{a}{r}\right)^4 B_2 \frac{\hat{\mathbf{e}}\cdot\mathbf{r}}{r}\left(\frac{\hat{\mathbf{e}}\cdot\mathbf{r}}{r}\frac{\mathbf{r}}{r} - \hat{\mathbf{e}}\right), \end{aligned} \tag{A.1}$$

where $r = |\mathbf{r}|$. Subtracting $\frac{2}{3}B_1\hat{\mathbf{e}}$ from this gives the flow fields shown in figure 3.

## References

[1] Purcell E M 1977 *Am. J. Phys.* **45** 3
[2] Brennen C and Winet H 1977 *Annu. Rev. Fluid Mech.* **9** 339–98
[3] Lighthill J 1952 *Commun. Pure. Appl. Math.* **5** 109–18
[4] Blake J R 1971 *J. Fluid Mech.* **46** 199–208
[5] Ishikawa T, Simmonds M P and Pedley T J 2006 *J. Fluid Mech.* **568** 119
[6] Ishikawa T and Pedley T J 2008 *Phys. Rev. Lett.* **100** 088103
[7] Ehlers K M, Samuel A D T, Berg H C and Montgomery R 1996 *Proc. Natl Acad. Sci.* **93** 8340–3
[8] Leshansky A M, Kenneth O, Gat O and Avron J E 2007 *New J. Phys.* **9** 145
[9] Gauger E M and Stark H 2006 *Phys. Rev.* E **74** 021907
[10] Wada H and Netz R R 2007 *Phys. Rev. Lett.* **99** 108102
[11] Lowe C P 2003 *Trans. R. Soc. Lond.* B **358** 1543
[12] Lagomarsino M C, Capuani F and Lowe C P 2003 *J. Theor. Biol.* **224** 215
[13] Earl D J, Pooley C M, Ryder J F, Bredberg I and Yeomans J M 2007 *J. Chem. Phys.* **126** 064703
[14] Najafi A and Golestanian R 2004 *Phys. Rev.* E **69** 062901
[15] Elgeti J 2006 Sperm and Cilia Dynamics *PhD Thesis* University of Köln
[16] Lobaskin V, Lobaskin D and Kulić I M 2008 *Eur. Phys. J. Spec. Top.* **157** 149–56
[17] Malevanets A and Kapral R 1999 *J. Chem. Phys.* **110** 8605
[18] Malevanets A and Kapral R 2000 *J. Chem. Phys.* **112** 7260

[19] Kikuchi N, Pooley C M, Ryder J F and Yeomans J M 2003 *J. Chem. Phys.* **119** 6388
[20] Ihle T, Tüzel E and Kroll D M 2004 *Phys. Rev.* E **70** 03570
[21] Götze I O, Noguchi H and Gompper G 2007 *Phys. Rev.* E **76** 046705
[22] Padding J T, Wysocki A, Löwen H and Louis A A 2005 *J. Phys.: Condens. Matter* **17** S3393
[23] Lamura A, Gompper G, Ihle T and Kroll D M 2001 *Europhys. Lett.* **56** 319–25
[24] Doi M and Edwards S F 1986 *The Theory of Polymer Dynamics* (Oxford: Oxford University Press)
[25] Howse J R, Jones R A L, Ryan A J, Gough T, Vafabakhsh R and Golestanian R 2007 *Phys. Rev. Lett.* **99** 048102